Multiconfigurational Surface Hopping: A Time-Dependent Variational Approach with Momentum-Jump Trajectories

Guijie Li,[#] *Zhecun Shi*,[#] *Lei Huang*, and *Linjun Wang**

Key Laboratory of Excited-State Materials of Zhejiang Province, Department of Chemistry, Zhejiang University, Hangzhou 310058, China

ABSTRACT: The Ehrenfest mean field dynamics and trajectory surface hopping have been widely used in nonadiabatic dynamics simulations. Based on the time-dependent variational principle (TDVP), the multiconfigurational Ehrenfest (MCE) method has also been developed and can be regarded as a multiconfigurational extension of the traditional Ehrenfest dynamics. However, it is not straightforward to apply the TDVP to surface hopping trajectories because there exists momentum jump during surface hops. To solve this problem, we here propose a multiconfigurational surface hopping (MCSH) method, where continuous momenta are obtained by linear interpolation and the interpolated trajectories are used to construct the basis functions for TDVP in a post-processing manner. As demonstrated in a series of representative spin-boson models, MCSH achieves high accuracy with only several hundred trajectory bases and can uniformly improve the performance of surface hopping. In principle, MCSH can be combined with all kinds of mixed quantum-classical trajectories, and thus has the potential to properly describe general nonadiabatic dynamics.

1. INTRODUCTION

Nonadiabatic dynamics involves significant coupling between quantum particles and the environment, which is ubiquitous in many different research fields, such as condensed-matter physics,[1–3] photochemistry,[4–6] biology,[7–9] and materials science.[10–14] Appropriate methods are required to attain a reliable description of these nonadiabatic processes. Although fully quantum dynamics methods give highly accurate results, the problem of the "curse of dimensionality" has prevented them from being applied to large complex systems.[15–27] Since heavy nuclei often behave classically, treating all the degrees of freedom with quantum mechanics is unnecessary. As a result, the mixed quantum-classical dynamics (MQCD) methods can potentially achieve good accuracy and efficiency through properly dividing the whole system into quantum and classical subsystems and describing them with different levels of theory. As representative independent-trajectory MQCD methods, the trajectory surface hopping (TSH)[28] and Ehrenfest mean field (EMF)[29] methods have been widely employed for nonadiabatic dynamics simulations due to their ease of implementation and compatibility with electronic structure calculations.[30–45] In particular, many theoretical advances have been made to further improve the performance of TSH and EMF.[46–52]

The accuracy of MQCD simulations relies on the description of quantum-classical (i.e., electron-nuclei) correlation. In the EMF dynamics, an effective wave packet (WP) moving on the average potential energy surface (PES) is used to describe the dynamics, and the quantum-classical correlation is governed by a simple mean field Hamiltonian. However, the mean field approximation has intrinsic problems. For instance, the EMF

dynamics cannot reproduce the spatial splitting of WPs and obtain all the dynamics channels. In TSH, the nuclei always move on an active adiabatic PES with stochastic transitions between different PESs. Although the active states in the trajectory ensemble better reproduces the fully quantum dynamics, the time evolution of the electronic wave function along each trajectory remains coherent due to the absence of intertrajectory correlation. In recent years, such an overcoherence problem has attracted extensive attention, and significant improvements have been made based on decoherence time formulas,[53–61] pure dephasing,[62] quantum measurement,[63,64] exact factorization,[65–68] trajectory branching,[69–79] and so on.

The time-dependent variational principle (TDVP) provides effective solutions to the time-dependent Schrödinger equation (TDSE) as long as the basis set is complete enough for the given problem.[80,81] Shalashilin and coworkers proposed two versions of the multiconfigurational Ehrenfest (MCE) method with different ansatz based on EMF-like time-dependent trajectory basis functions (TBFs) defined by coherent states (CSs).[82,83] In the first version of MCE (MCEv1),[82] the TDVP is carried out "on the fly" in the complete vibronic amplitude manifold. Although high accuracy can be attained, the TBFs must be generated along with the time-dependent evolution of amplitudes. In comparison, the second version of MCE (MCEv2) adopts a "post-processing" approach.[83] Namely, the amplitudes are only coupled within individual configurations, and thus the variation of configuration coefficients can be realized after the variation of vibronic amplitudes. Although high efficiency can be realized, it is more difficult to converge to the exact quantum solution because there is no coupling between vibronic

amplitudes in different configurations.

In principle, the TDVP can be applied to any basis set. It is well known that the trajectories by TSH are often better than those by EMF because TSH can describe WP splitting and has better detailed balance. Therefore, we may expect that using TSH instead of EMF to generate the TBFs for TDVP may achieve better performance. To this end, we here propose a multiconfigurational surface hopping (MCSH) method. Linear interpolation is utilized to solve the momentum jump problem due to surface hops, and the interpolated TSH trajectories are taken as the new TBFs embedded into the MCEv1 ansatz to achieve a "post-processing" variation of the configurations. To show that MCSH could compensate for the insufficient quantum description of nuclei in TSH simulations and improve the accuracy, MCSH is systematically benchmarked in spin-boson models using the exact quantum solutions and FSSH results as references.

2. THEORY

A. Fewest Switches Surface Hopping

In nonadiabatic dynamics simulations with the traditional fewest switches surface hopping (FSSH),[28] the adiabatic representation is generally preferred. For a system composed of both electronic and nuclear degrees of freedom, the Hamiltonian reads

$$\hat{H} = \hat{T}_n + \hat{H}_{el}(\boldsymbol{r};\boldsymbol{q}), \tag{1}$$

where $\boldsymbol{r}$ and $\boldsymbol{q}$ are the electronic and nuclear coordinates, $\hat{T}_n$ and $\hat{H}_{el}(\boldsymbol{r};\boldsymbol{q})$ are the nuclear kinetic energy operator and the electronic Hamiltonian, respectively. In each FSSH trajectory, the initial electronic wave function, active state, nuclear coordinates

and momenta are set according to the problem under investigation. At each time t, by solving the time-independent Schrödinger equation,

$$\hat{H}_{el}(\boldsymbol{r};\boldsymbol{q}(t))\left|\phi_i(\boldsymbol{r};\boldsymbol{q}(t))\right\rangle = E_i(\boldsymbol{q}(t))\left|\phi_i(\boldsymbol{r};\boldsymbol{q}(t))\right\rangle, \tag{2}$$

we can obtain all the adiabatic eigenenergies $\{E_i(\boldsymbol{q}(t))\}$ and the corresponding eigenstates $\{|\phi_i(\boldsymbol{r};\boldsymbol{q}(t))\rangle\}$ at the nuclear configuration $\boldsymbol{q}(t)$. The nuclear motion on the active PES a follows the classical Newton equation,

$$\frac{d\boldsymbol{p}}{dt} = -\nabla_{\boldsymbol{q}} E_a, \tag{3}$$

where $\boldsymbol{p}$ indicates the nuclear momenta and E_a is energy of the active PES. The electronic wave function $|\psi(\boldsymbol{r},t)\rangle$ can be linearly expanded as

$$|\psi(\boldsymbol{r},t)\rangle = \sum_i c_i(t)\left|\phi_i(\boldsymbol{r};\boldsymbol{q}(t))\right\rangle, \tag{4}$$

where $\{c_i(t)\}$ are expansion coefficients. To propagate the electronic wave function, eq. 4 is substituted into the time-dependent Schrödinger equation,

$$i\hbar\frac{\partial|\psi(\boldsymbol{r},t)\rangle}{\partial t} = \hat{H}_{el}(\boldsymbol{r};\boldsymbol{q}(t))|\psi(\boldsymbol{r},t)\rangle, \tag{5}$$

which results in

$$i\hbar\frac{d}{dt}c_i = c_i E_i(\boldsymbol{q}) - i\hbar\sum_j c_j \dot{\boldsymbol{q}}\cdot\boldsymbol{d}_{ij}(\boldsymbol{q}), \tag{6}$$

where $\boldsymbol{d}_{ij}(\boldsymbol{q}) = \left\langle\phi_i(\boldsymbol{r};\boldsymbol{q})\left|\nabla_{\boldsymbol{q}}\phi_j(\boldsymbol{r};\boldsymbol{q})\right.\right\rangle$ is the nonadiabatic coupling vector between adiabatic states i and j. The adiabatic electronic populations are calculated as $\rho_{ii} = c_i c_i^*$. Based on eq. 6, the time evolution of the population on each electronic state i is

$$\frac{d\rho_{ii}}{dt} = \sum_{j(\neq i)} b_{ij}, \tag{7}$$

where $b_{ij} = -2\,\mathrm{Re}(\rho_{ij}^*\dot{\boldsymbol{q}}\cdot\boldsymbol{d}_{ij})$. In the standard FSSH, during each time interval [t, t + dt],

the hopping probability from the active state a to another state k is defined as

$$g_{ak} = -\frac{b_{ak}\mathrm{d}t}{\rho_{aa}}, \tag{8}$$

which is reset to zero if negative. At each time step, we generate a uniformly distributed random number $\xi \in [0,1]$, and the surface hop from a to k is assigned if $\sum_{i=1}^{k-1} g_{ai} < \xi \leq \sum_{i=1}^{k} g_{ai}$, and the nuclear momenta are rescaled along the direction of $\boldsymbol{d}_{ak}$ to conserve the total energy. If the energy conservation is violated, frustrated hopping happens and the surface hop is canceled. The above steps are repeated and a swarm of independent trajectories are obtained until the predefined criterion is satisfied.

B. MCEv1 and MCEv2

As an extension of the traditional Ehrenfest dynamics, Shalashilin and coworkers proposed two versions of the MCE method for quantum dynamics, namely MCEv1[82] and MCEv2.[83] In both versions, an Ehrenfest configuration is represented as

$$\left|\psi(t)\right\rangle = \left|\phi_{\text{system}}(t)\right\rangle \left|\mathbf{z}_{\text{bath}}(t)\right\rangle, \tag{9}$$

where $\left|\phi_{\text{system}}(t)\right\rangle$ is the wave function of the electronic system, and $\left|\mathbf{z}_{\text{bath}}(t)\right\rangle$ is the multidimensional wave function of the nuclear bath. If there are M vibrational modes in the bath, we can express $\left|\mathbf{z}_{\text{bath}}(t)\right\rangle$ as the product of individual CS for each mode m,

$$\left|\mathbf{z}_{bath}(t)\right\rangle = \prod_{m=1}^{M} \left|z^{m}(t)\right\rangle. \tag{10}$$

Here, each one-dimensional CS $\left|z^{m}(t)\right\rangle$ is a frozen Gaussian WP with fixed width γ under the coordinate representation,

$$\left\langle x \middle| z^{m} \right\rangle = \left(\frac{\gamma}{\pi}\right)^{1/4} \exp\left[-\frac{\gamma}{2}(x-q^{m})^{2} + ip^{m}(x-q^{m}) + \frac{ip^{m}q^{m}}{2}\right], \tag{11}$$

where q^m and p^m are the expectation value of the coordinate and momentum for mode

m. Note that $\left|z^m(t)\right\rangle$ is the eigenstate of the annihilation operator for the m-th harmonic vibration, and the eigenvalue z^m is expressed as

$$z^m = \left(\frac{\gamma}{2}\right)^{1/2} q^m + \frac{i}{\hbar}\left(\frac{1}{2\gamma}\right)^{1/2} p^m . \tag{12}$$

Different ansatzes are utilized in MCEv1 and MCEv2 to realize a multiconfigurational description of the system-bath wave function. Namely, MCEv1 uses

$$\left|\Psi(t)\right\rangle = \sum_{j=1}^{N}\left|\psi_j(t)\right\rangle = \sum_{j=1}^{N}\sum_{s} a_j^{(s)}(t)\left|\mathbf{z}_j(t)\right\rangle\left|s\right\rangle, \tag{13}$$

and MCEv2 takes the form

$$\left|\Psi(t)\right\rangle = \sum_{j=1}^{N} C_j(t)\sum_{s} a_j^{(s)}(t)\left|\mathbf{z}_j(t)\right\rangle\left|s\right\rangle = \sum_{j=1}^{N} C_j(t)\left|\psi_j(t)\right\rangle, \tag{14}$$

where $\left\{\left|s\right\rangle\right\}$ is an orthonormal diabatic basis of the system and does not rely on the bath variables. In MCEv1, all the vibronic amplitudes $\{a_j^{(s)}\}$ are coupled to each other and the whole wave function is normalized (i.e., $\left\langle\Psi\middle|\Psi\right\rangle = 1$). The equation of motion for $\{a_j^{(s)}\}$ can be obtained from the TDVP,

$$\sum_{j=1}^{N} i\hbar\left\langle\mathbf{z}_l\middle|\mathbf{z}_j\right\rangle\dot{a}_j^{(s)} = \sum_{j=1}^{N}\sum_{s'}\left\langle\mathbf{z}_l\middle|\hat{H}_{ss'}\middle|\mathbf{z}_j\right\rangle a_j^{(s')} - \sum_{j=1}^{N} i\hbar\left\langle\mathbf{z}_l\middle|\dot{\mathbf{z}}_j\right\rangle a_j^{(s)}, \tag{15}$$

where $\hat{H}_{ss'} = \left\langle s\middle|\hat{H}\middle|s'\right\rangle$ are matrix elements of the total system-bath Hamiltonian. In MCEv2, each configuration j is normalized, i.e., $\left\langle\psi_j(t)\middle|\psi_j(t)\right\rangle = 1$. By applying the TDVP to each configuration j in eq. 14, we obtain

$$i\hbar\dot{a}_j^{(s)} = \sum_{s'}\left\langle\mathbf{z}_j\middle|\hat{H}_{ss'}\middle|\mathbf{z}_j\right\rangle a_j^{(s')} - i\hbar\left\langle\mathbf{z}_j\middle|\dot{\mathbf{z}}_j\right\rangle a_j^{(s)} . \tag{16}$$

Then, the configuration interactions are described by the coupled equations

$$\sum_{j=1}^{N} i\hbar\left\langle\psi_l\middle|\psi_j\right\rangle\dot{C}_j = \sum_{j=1}^{N}\left\langle\psi_l\middle|\hat{H}\middle|\psi_j\right\rangle C_j - \sum_{j=1}^{N} i\hbar\left\langle\psi_l\middle|\dot{\psi}_j\right\rangle C_j . \tag{17}$$

Both MCEv1 and MCEv2 use Ehrenfest-like trajectories propagated through

$$i\hbar\dot{\mathbf{z}}_j = -\frac{\partial\left\langle \mathbf{z}_j \middle| \hat{H}_j^{MF} \middle| \mathbf{z}_j \right\rangle}{\partial \mathbf{z}_j^*}, \tag{18}$$

where $\hat{H}_j^{MF}$ is the corresponding mean field Hamiltonian operator defined as

$$\hat{H}_j^{MF} = \frac{\sum_{s,s'} a_j^{(s)*} a_j^{(s')} \hat{H}_{ss'}}{\sum_s \left| a_j^{(s)} \right|^2}. \tag{19}$$

Thereby, the most significant difference between the two MCE ansatzes is the description of configuration interactions. The fully correlated configurations in MCEv1 can explore a larger configuration space but must propagate simultaneously. The configurations in MCEv2 are independent and interact with each other in a post-processing manner, making MCEv2 more suitable for *ab initio* quantum dynamics.

C. Multiconfigurational Surface Hopping

Since the "on the fly" ansatz in MCEv1 can well characterize the correlation between configurations, high accuracy is generally achieved while losing a certain extent of flexibility in choosing the time-dependent trajectory basis. In contrast, the MCEv2 ansatz in the "post-processing" form is based on independent TBFs, achieving high efficiency while sacrificing its accuracy in some cases. As TSH has proven its reliability in many studies, we may expect that trajectories produced by TSH dynamics may be better than those by EMF. Therefore, we here propose a novel MCSH method based on FSSH and MCEv1. In detail, we embed independent trajectories of FSSH into the MCEv1 ansatz to achieve the "post-processing" variation of multiconfigurational correlations and describe the entangled system-bath dynamics.

In MCEv1, the time evolution of the vibronic amplitudes (i.e., eq. 15) describes the multiconfigurational correlation and the Ehrenfest trajectories (i.e., eq. 18) are used

to define the CSs. As the CS used in the multiconfigurational dynamics is a frozen Gaussian WP defined by the complex vector $\mathbf{z}$ which can be considered as a point in the phase space, we can maintain the form of eq. 15 and propagate surface hopping trajectories in the adiabatic representation to obtain $\left\{\left|\mathbf{z}_j\right\rangle\right\}$ and $\left\{\left|\dot{\mathbf{z}}_j\right\rangle\right\}$. Instead of using eq. 18, $\mathbf{z}_j$ and its time derivative $\dot{\mathbf{z}}_j$ for the j-th CS are given by

$$\mathbf{z}_j = \left(\frac{\gamma}{2}\right)^{1/2} \boldsymbol{q}_{SH,j} + \frac{i}{\hbar}\left(\frac{1}{2\gamma}\right)^{1/2} \boldsymbol{p}_{SH,j}, \tag{20}$$

$$\dot{\mathbf{z}}_j = \left(\frac{\gamma}{2}\right)^{1/2} \dot{\boldsymbol{q}}_{SH,j} + \frac{i}{\hbar}\left(\frac{1}{2\gamma}\right)^{1/2} \dot{\boldsymbol{p}}_{SH,j}, \tag{21}$$

where $\boldsymbol{q}_{SH,j}$ and $\boldsymbol{p}_{SH,j}$ are the nuclear coordinates and momenta in the j-th surface hopping trajectory. Eqs. 20 and 21 are substituted into eq. 15 to describe the configuration interaction and realize the post-processing variation of the independent surface hopping trajectories.

The step-by-step outline of the MCSH algorithm is as follows:

(1) At time zero, N_{conf} FSSH trajectories are generated and their initial conditions are set according to the problem under investigation.

(2) At each time t, the nuclei and electrons for each FSSH trajectory are evolved according to eqs. 3 and 6 in the adiabatic representation, respectively.

(3) The N_{conf} CSs are constructed and their time derivatives are calculated using eqs. 20 and 21 based on the corresponding FSSH trajectory. The vibronic amplitudes are propagated by solving eq. 15.

(4) When a surface hop occurs in a FSSH trajectory, the corresponding TBF becomes discontinuous due to the momentum jump. To solve this problem, we here

introduce the linear interpolation of nuclear coordinates and momenta. As shown in Figure 1, suppose the active state and the nuclear momenta change during the time interval [t - dt, t]. We reset the nuclear coordinates and momenta as well as the configuration amplitudes to those at the previous time step t – dt, and then all the involved quantities are linearly interpolated between t - dt and t. Suppose N_{interp} is the number of interpolation steps. The linear interpolation is equivalent to using a smaller time step size of dt/N_{interp} to evolve the nuclear momenta $\boldsymbol{p}_{\text{interp},j}$ and coordinates $\boldsymbol{q}_{\text{interp},j}$ along each trajectory j with

$$\dot{\boldsymbol{p}}_{\text{interp},j} = \frac{\boldsymbol{p}_{SH,j}(t) - \boldsymbol{p}_{SH,j}(t-\mathrm{d}t)}{\mathrm{d}t}, \tag{22}$$

$$\dot{\boldsymbol{q}}_{\text{interp},j} = \frac{\boldsymbol{q}_{SH,j}(t) - \boldsymbol{q}_{SH,j}(t-\mathrm{d}t)}{\mathrm{d}t}, \tag{23}$$

and the variation of vibronic amplitudes still follows eq. 15.

(5) Steps 2 – 4 are repeated until the predefined criterion is achieved.

3. RESULTS AND DISCUSSION

A. Spin-Boson Model

The spin-boson model has been widely utilized to study the nonadiabatic dynamics in condensed phase.[84] The Hamiltonian is expressed as $\hat{H} = \hat{H}_s + \hat{H}_b + \hat{H}_{sb}$. Here, $\hat{H}_s$ is the two-level system Hamiltonian with energy bias ε and constant coupling Δ between the two diabatic electronic states,

$$\hat{H}_s = \varepsilon\hat{\sigma}_z + \Delta\hat{\sigma}_x, \tag{24}$$

where $\hat{\sigma}_x$ and $\hat{\sigma}_z$ are the corresponding Pauli operators. $\hat{H}_b$ and $\hat{H}_{sb}$ are respectively Hamiltonians of the bath composed of M harmonic oscillators and the

system-bath coupling,

$$\hat{H}_b = \sum_m^M \omega^m \left(\hat{b}^{m\dagger} \hat{b}^m + \frac{1}{2} \right), \tag{25}$$

$$\hat{H}_{sb} = \hat{\sigma}_z \sum_m^M \frac{c^m}{\sqrt{2\omega^m}} \left(\hat{b}^{m\dagger} + \hat{b}^m \right), \tag{26}$$

where $\hat{b}^{m\dagger}$ and $\hat{b}^m$ are the bosonic creation and annihilation operators for the m-th harmonic oscillator, respectively. In this study, we adopt the Ohmic spectral density to depict the system-bath coupling,[85]

$$J(\omega) = \frac{\pi}{2} \alpha_k \omega e^{-\omega/\omega_c}, \tag{27}$$

where α_k is the Kondo parameter related to the system-bath coupling strength, and ω_c is the characteristic frequency. Note that the continuum spectral density can be generally discretized as

$$J(\omega) = \frac{\pi}{2} \sum_m \frac{(c^m)^2}{\omega^m} \delta(\omega - \omega^m), \tag{28}$$

where $\{c^m\}$ are the coupling parameters and $\{\omega^m\}$ are the bath frequencies. To express eq. 27 with eq. 28, we may adopt the widely used approach, which could accurately reproduce the reorganization energy.[86] Namely, $\{c^m\}$ and $\{\omega^m\}$ are calculated as

$$c^m = \omega^m \sqrt{\frac{\alpha_k \omega_c}{M} (1 - e^{-\omega_{max}/\omega_c})}, \tag{29}$$

$$\omega^m = -\omega_c \ln \left[1 - \frac{j}{M} \left(1 - e^{-\omega_{max}/\omega_c} \right) \right], \tag{30}$$

where ω_{max} is generally set as $5\omega_c$.

B. Initial Condition

The multiconfigurational dynamics described above is only applicable at zero temperature. To realize finite-temperature simulations, we here adopt a Monte Carlo method to set initial conditions.[87,88] Suppose the initial density matrix of the total system is

$$\hat{\rho}_{tot}(0) = \hat{\rho}_b^{eq} \otimes \hat{\rho}_s(0), \tag{31}$$

where $\hat{\rho}_s(0) \equiv |1\rangle\langle 1|$ is the initial reduced density matrix of the system subspace , and $\hat{\rho}_b^{eq}$ is the equilibrium bath density operator at temperature T, i.e., $\hat{\rho}_b^{eq} = e^{-\beta \hat{H}_b'} / Z$. Here, $\beta = 1/(k_b T)$ is the inverse temperature divided by the Boltzmann constant k_b and Z is the partition function of the bath, $\hat{H}_b'$ is set as $\hat{H}_b$ and $\hat{H}_b + \sum_m c^m (\hat{b}^{m\dagger} + \hat{b}^m)/\sqrt{2\omega^m}$ for the bare local state and the dressed local state cases, respectively. In the CS representation, $\hat{\rho}_b^{eq}$ can be exactly written as the product of one-dimensional density operators,[87,88]

$$\hat{\rho}_b^{eq} = \int \frac{d^2\mathbf{z}_{\text{init}}}{\pi^M} |\mathbf{z}_{\text{init}}\rangle \rho_b(\mathbf{z}_{\text{init}}) \langle \mathbf{z}_{\text{init}}| = \prod_{m=1}^{M} \int \frac{d^2 z_{init}^m}{\pi} |z_{\text{init}}^m\rangle \rho_b(z_{\text{init}}^m) \langle z_{\text{init}}^m|, \tag{32}$$

where $|z_{\text{init}}^m\rangle$ is the CS for each mode m in the bath. Eq. 32 can be regarded as sampling of z_{init}^m from the Gaussian distribution,[89]

$$\rho_b(z_{\text{init}}^m) = \frac{e^{\beta\omega^m} - 1}{\pi} e^{-\left[(\text{Re}(z_{\text{init}}^m)+\zeta_x)^2 + (\text{Im}(z_{\text{init}}^m)+\zeta_y)^2\right](e^{\beta\omega^m}-1)}. \tag{33}$$

It is worth noting that we need to generate a set of N_{rep} $|\mathbf{z}_{\text{init}}\rangle$ with different initial conditions of bath based on the quantum Boltzmann distribution and propagate the corresponding wave function independently to get the converged results.[82] To realize multiconfigurational dynamics, each $|\mathbf{z}_{\text{init}}\rangle$ should be expanded using the CS basis set $\{|\mathbf{z}_j\rangle\}$, which is sampled from a Gaussian distribution biased to the center of $|z_{\text{init}}^m\rangle$ to

cover the initial wave function of bath $|\mathbf{z}_{\text{init}}\rangle$,[90]

$$F(z_j^m) \propto \exp(-\alpha_{\text{comp}} | z_j^m - z_{\text{init}}^m |^2), \tag{34}$$

where α_{comp} is the compression parameter related to the density of the initial CS basis set. A large compression parameter corresponds to dense sampling, which can cover the initial bath wave function better and have a lower initial expansion error. In this study, we uniformly set $\alpha_{\text{comp}} = 2500$.

The initial wave function can be written as

$$|\Psi_0(0)\rangle = |\mathbf{z}_{\text{init}}\rangle\big(1|1\rangle + 0|2\rangle\big). \tag{35}$$

For the multiconfiguration expansion, we set the $a_j^{(2)} = 0$ for the initial wave function in MCSH to match the initial condition,

$$|\Psi(t=0)\rangle = \sum_{j=1}^{N} |\mathbf{z}_j\rangle\big(a_j^{(1)}|1\rangle + a_j^{(2)}|2\rangle\big) = \sum_{j=1}^{N} a_j^{(1)} |\mathbf{z}_j\rangle|1\rangle. \tag{36}$$

To decompose the initial wave function in the CS subspace, we define the error function $I = \big\| |\Psi\rangle - |\Psi_0\rangle \big\|^2$ and get the initial amplitudes $\{a_j^{(1)}\}$ by minimizing the expansion error. In MCSH, the initial momenta and coordinates of the FSSH trajectories are obtained according to the initial CSs. Moreover, we choose the initial active states randomly according to the adiabatic electronic populations after representation transformation. The time evolution of $|\mathbf{z}_{\text{init}}\rangle$ is described by the motion of the CS basis and their time-dependent amplitudes.

C. Numerical Results

The spin-boson models with different parameters have been widely utilized to represent different dynamical situations, and fully quantum dynamics results can be obtained. Thereby, they can be used to benchmark the performance of new nonadiabatic

dynamics methods. For simplicity and without loss of generality, we use the diabatic coupling Δ as the unit of energy. As listed in Table 1, we consider nine representative spin-boson models (i.e., SBM-1 ~ SBM-9),[16,86,91–93] which have included both symmetric ($\varepsilon = 0$) and asymmetric ($\varepsilon \neq 0$) cases at low and high temperatures starting from bare and dressed local states. The effective temperature $\beta\Delta$ is between 0.1 and 1000, the Kondo parameter α_k is in the range of 0.09 and 4, and the characteristic frequency ω_c/Δ is between 1 and 10. The MCEv1 and MCEv2 results are provided in the supporting information (SI). In all investigated systems, the MCSH results are much better than those of MCEv2. MCSH generally gives similar results as MCEv1, but performs better in some systems (see details in the SI). In the following discussions, we will focus on the performance of FSSH and MCSH. In Table 1, we also give the number trajectories in FSSH simulations (N_{traj}) and the number of configurations (N_{conf}) in MCSH calculations for each model. In these models, MCSH obtains converged results with only a few hundred configurations while FSSH needs thousands of trajectories.

It is well known that asymmetric models at low temperature are more difficult to deal with. Thereby, we first use SBM-1 as an illustration and explore the performance of MCSH with different N_{interp}. In Figure 2, we show the time-dependent population difference between the two diabatic electronic states with N_{interp} = 10, 20, 50, 100, 200, and 500. α_{comp} = 2500 gives $\langle\Psi|\Psi\rangle > 1-1\times10^{-6}$, implying that the initial wave function is perfectly expanded by the CS bases. For the exact quantum dynamics, the population gradually transfers from diabatic state $|1\rangle$ to the diabatic state $|2\rangle$. The results with different N_{interp} are highly consistent with the exact quantum results,

indicating that the MCSH results converge quickly with the choice of N_{interp}. Thereby, we have proved that the TDVP can be applied to momentum-jump trajectories with our linear interpolation approach, thus significantly expanding the possibility of using more accurate and efficient TBFs for MCSH simulations.

In Figure 3, we systematically compare the performance of FSSH, MCSH, MCEv1, and MCEv2 methods in SBM-1. It is apparent that FSSH only captures the first oscillation of the diabatic population difference and the equilibrium population is significantly overestimated. The MCEv2 results show excessive oscillations of the population difference although the oscillating phases are captured (see Figure S1). This may be attributed to the lack of WP splitting in the individual mean-field trajectories, and the uncorrelated mean-field configurations are insufficient to describe the system-bath coupling. Similar to MCEv1, our MCSH method reproduces the quantum results both in short-term and long-term dynamics. Thereby, the correlated variation of vibronic amplitudes is crucial to make improvements on FSSH trajectories.

Similar to MCSH, we can also embed the EMF[29] trajectories into the MCEv1 ansatz to get a post-processing method, which is named as multiconfigurational mean field (MCMF) dynamics. Compared with MCEv1, although MCMF is also based on Ehrenfest TBFs, MCMF belongs to the post-processing variation between independent TBFs. Compared with MCEv2, although MCMF is also based on the independent mean field TBFs, the vibronic amplitudes are fully correlated through the MCEv1 ansatz, that is, eq. 15 is used instead of eqs. 16 and 17. As shown in Figure 3, MCMF with the same N_{conf} gives too large long-term oscillations and population differences. Therefore, the

post-processing variation with mean field trajectories is indeed inferior to that with surface hopping trajectories, justifying our motivation of the MCSH method.

In Figure 4, we study SBM-2, which is a symmetric model at low temperature. In this case, both FSSH and MCSH give the same long-term populations for the two electronic states, indicating that both dynamics have reached thermal equilibrium in accord with the exact quantum dynamics. Although FSSH properly captures the oscillation phases, it underestimates the oscillation amplitudes. In contrast, MCSH gives almost identical populations as the quantum results. As shown in Figure S2, MCSH even better captures the oscillation phases than MCEv1 at $t\Delta > 9$, implying that using surface hopping trajectories for post-processing variation may have special advantages in certain long-time dynamics.

At lower temperatures, the nuclear quantum effect is more significant, and FSSH may have larger errors due to its MQCD feature. In Figure 5, we investigate SBM-3 at almost zero temperature. The detailed parameters are $\alpha_k = 1.5$, $\beta\Delta = 1000$, $\omega_c = 10\Delta$, $\varepsilon/\Delta = 0$ and $M = 500$. In this model, although there is no bias between the two electronic states, most of the long-time population is still on the initial state due to the extremely low temperature, large number of vibrational modes, high cutoff frequency, and strong system-bath coupling. The FSSH results show a quasi-linear decay and fail to reproduce the population localization. For MCEv2, the population localization is obtained, but there exist artificial population oscillations (see Figure S3). Encouragingly, MCSH still successfully reproduces the exact quantum results despite small deviations. In all the three low-temperature models (i.e., SBM-1, SBM-2 and SBM-3) investigated above,

MCSH consistently shows high performance and makes significant improvements compared with FSSH. This indicates that the surface hopping trajectories combined with the "post-processing" variation of correlated vibronic amplitudes can well describe the nonadiabatic dynamics in complex systems.

We also examine spin-boson models at high temperatures. In Figure 6, we show the time-dependent diabatic population difference in the symmetric SBM-4 model. The exact quantum results exhibit some oscillations during the decay dynamics. Although at a relatively high temperature, a stronger system-bath coupling is also present in SBM-4, and thus FSSH still shows some errors. Namely, FSSH only tracks the first part of the decay and the population decreases monotonically with time. In contrast, MCSH closely reproduces the time evolution of exact populations, which again shows that the "post-processing" variation of surface hopping trajectories is reliable.

SBM-5 is an asymmetric model at high temperature. In this case, the nuclear quantum effect of the bath is relatively weak. As shown in Figure 7, the quantum results experience a few small oscillations and then show a long-term asymptotic decay. It is evident that FSSH performs quite well as other methods. In terms of details, although all investigated methods reproduce the oscillation features and subsequent decay over time of the population difference, MCSH shows the best performance. Therefore, regardless of the performance of FSSH, the "post-processing" variation of correlated vibronic amplitudes based on surface hopping TBFs can always provide an accurate description of the system-bath entangled dynamics.

To give a more comprehensive evaluation of the performance of MCSH, we study

four additional models (i.e., SBM-6, SBM-7, SBM-8, and SBM-9), which have also been extensively studied in the literature (see Figure S6). In the low-temperature models, there exist coherent oscillations of the population difference in the exact quantum dynamics, and MCEv2 generally shows too large oscillation amplitudes (see Figures S6a and S6b). While FSSH exhibits different performance in different models, it well reproduces the coherent oscillation of population in SBM-7 (see Figure S6b) and the incoherent damping of population in SBM-9 (see Figure S6d). In contrast, MCSH gives much stable results and is generally more consistent with the exact results. In particular, MCSH even shows better long-time performance than MCEv1 in SBM-7 (see Figure S6b). Note that SBM-8 presents a significant system-bath coupling and energy bias between the two electronic states. As a result, the decoherence in this system is much stronger than other cases. As the ansatz in this study possesses a coherent superposition of vibronic amplitudes, it may be not suitable to efficiently describe such strong decoherence. Therefore, this model is challenging for all investigated methods, which have shown similar results (see Figure S6c) and may need a large number of configurations to obtain the exact results.

4. CONCLUSION

In summary, we have proposed a novel MCSH method for nonadiabatic dynamics simulations. The correlation between configurations based on independent and interpolated surface hopping TBFs has been realized, and the advantages of both multiconfigurational and surface hopping dynamics have been taken. We have benchmarked the performance of MCSH in a series of spin-boson models, where

complex dynamics emerges from the interaction between nuclear and electronic degrees of freedom and can be easily tuned by the model parameters. MCSH uses linear interpolation to solve the momentum-jump problem due to surface hops, and the results converge rapidly with the number of interpolations. MCSH has provided results that are in high agreement with the exact solutions and systematically improves over FSSH. The surface hopping TBFs with momentum jump can be regarded as an efficient choice of basis set and open a new perspective for multiconfigurational dynamics. In addition, due to the independence of surface hopping trajectories, we can make parallel computing to get the TBFs, which is vital for improving the efficiency of nonadiabatic dynamic simulations. From this perspective, our MCSH method has great potential to be combined with electronic structure calculations for realistic applications.

Finally, the choices of TBFs are essential for MCSH and merit further discussion. Better trajectories might make the time-dependent variation of the vibronic amplitudes converge more quickly with respect to the number of TBFs.[94,95] Generating better trajectories with other methods instead of the traditional surface hopping scheme needs further investigations. For instance, the global flux surface hopping (GFSH) method is a useful variant of FSSH. GFSH not only has higher performance in superexchange dynamics but also shows better detailed balance.[96,97] In addition, GFSH is more suitable for nonadiabatic dynamic simulations with complex surface crossings because its hopping probabilities do not rely on the nonadiabatic couplings.[98] Therefore, the GFSH trajectories can be used as TBFs in MCSH simulations to study the nonadiabatic dynamics in more complex systems. These studies are currently underway.

AUTHOR INFORMATION

[#]These authors contributed equally to this work.

Corresponding Author

*E-mail: ljwang@zju.edu.cn.

Author Contributions

The manuscript was written through the contributions of all authors. All authors have approved the final version of the manuscript.

Notes

The authors declare no competing financial interests.

ACKNOWLEDGMENT

We acknowledge the supports from the National Natural Science Foundation of China (Grant No. 22273082) and the High-Performance Computing Center in the Department of Chemistry, Zhejiang University.

ASSOCIATED CONTENT

Supporting Information

We give the results of MCEv2 and MCEv1 for the investigated spin-boson models.

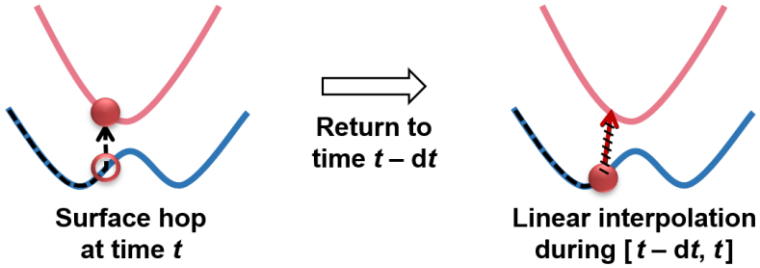

Figure 1. Schematic representation of the linear interpolation of nuclear momenta in MCSH when a surface hop occurs. The two adiabatic PESs are shown by light blue and light red solid lines, respectively. The nuclear trajectory on the active PES is represented by the black dashed line. The movement directions of the nuclei are marked with arrows.

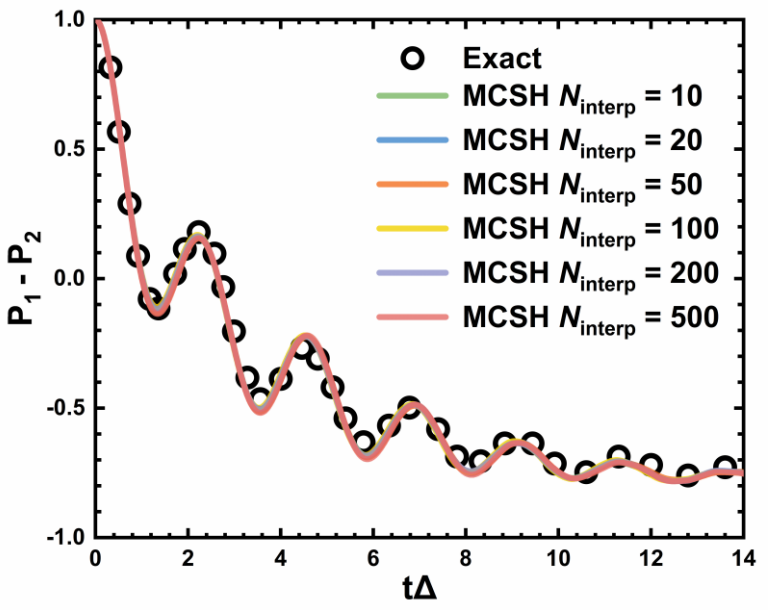

Figure 2. Diabatic population difference as a function of time obtained by MCSH with different numbers of interpolation points N_{interp} for the SBM-1 asymmetric spin-boson model at low temperature. The exact quantum solutions are shown by black open circles. The MCSH results with different N_{interp} are represented by solid lines in different colors.

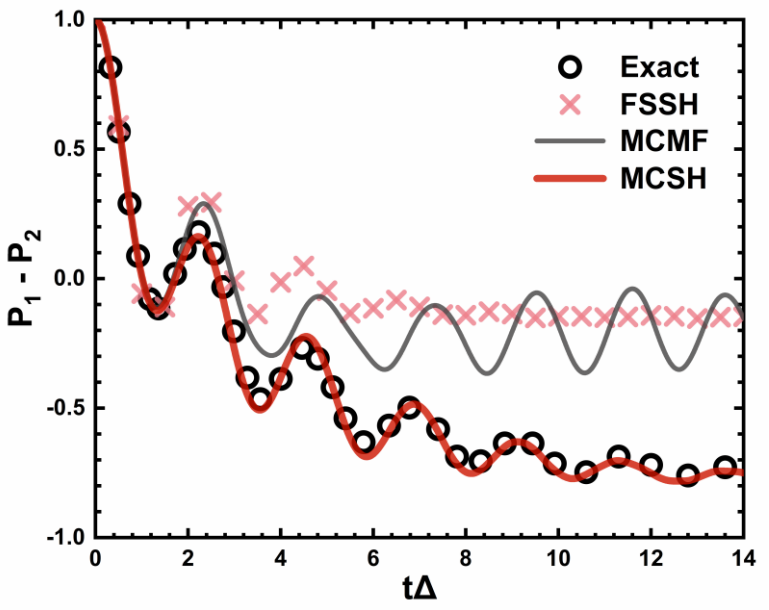

Figure 3. Diabatic population difference as a function of time for the SBM-1 asymmetric spin-boson model at low temperature. The results of exact quantum dynamics, FSSH, MCMF, and MCSH are shown by black open circles, light red crosses, grey solid lines, and dark red solid lines, respectively.

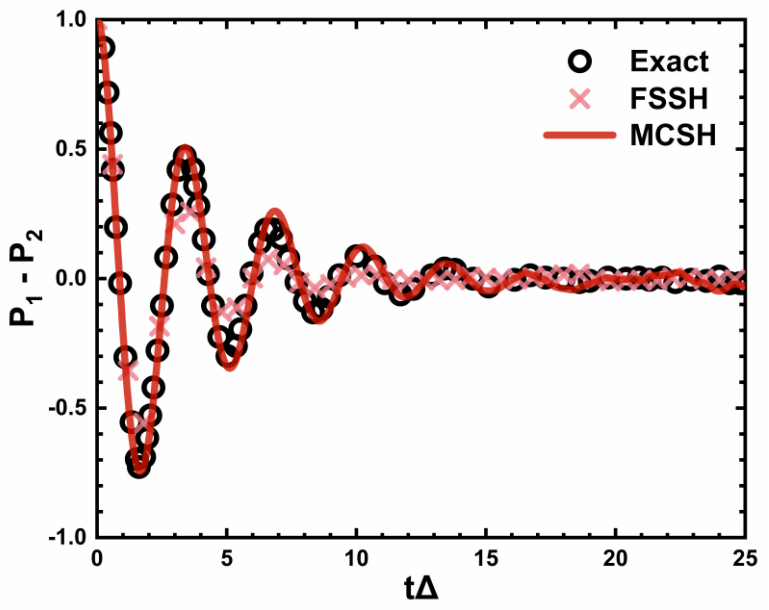

Figure 4. Diabatic population difference as a function of time for the SBM-2 symmetric spin-boson model at low temperature. The exact quantum solutions are shown by black open circles. The results of FSSH and MCSH are represented by the same styles as those in Figure 3.

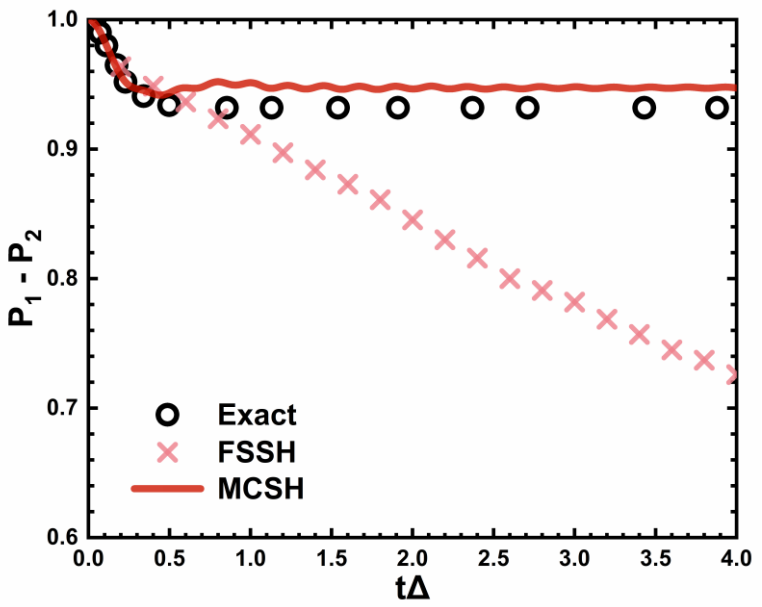

Figure 5. Diabatic population difference as a function of time for the SBM-3 symmetric spin-boson model at almost zero temperature. The exact quantum solutions are shown by black open circles. The results of FSSH and MCSH are represented as the same styles as those in Figure 3.

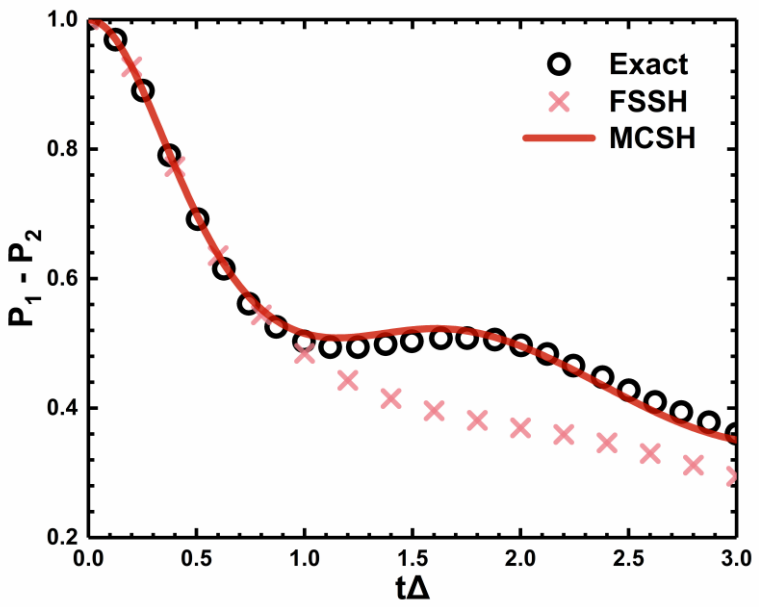

Figure 6. Diabatic population difference as a function of time for the SBM-4 symmetric spin-boson model at high temperature. The exact quantum solutions are shown by black open circles. The results of FSSH and MCSH are represented as the same styles as those in Figure 3.

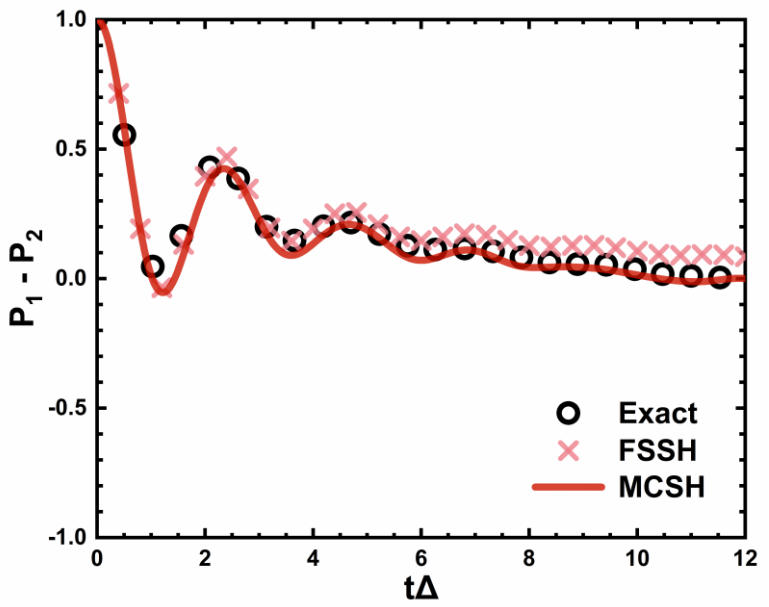

Figure 7. Diabatic population difference as a function of time for the SBM-5 asymmetric spin-boson model at high temperature. The exact quantum solutions are shown by black open circles. The results of FSSH and MCSH are represented as the same styles as those in Figure 3.

Table 1. Summary of the parameters, the number of trajectories N_{traj} in FSSH simulations, the number of configurations N_{conf} in MCSH calculations and the initial bath state for all investigated spin-boson models. N_{conf} in MCEv1, MCEv2, and MCMF are the same as that of in MCSH.The initial nuclear momenta and coordinates of the bath are sampled by the Wigner distribution in FSSH simulations.

Model	α_k	$\beta\Delta$	ω_c/Δ	ε/Δ	M	FSSH N_{traj}	MCSH N_{conf}	$\hat{\rho}_b^{eq}$
SBM-1	0.1	5	7.5	1	50	5000	100	bare local state
SBM-2	0.1	5	7.5	0	60	5000	100	bare local state
SBM-3	1.5	1000	10	0	500	1000	100	bare local state
SBM-4	2	1	1	0	100	10000	100	dressed local state
SBM-5	0.1	0.25	1	1	100	10000	100	dressed local state
SBM-6	0.1	5	2.5	1	100	5000	200	dressed local state
SBM-7	0.09	5	2.5	0	100	5000	100	dressed local state
SBM-8	4	0.1	2	5	100	10000	100	dressed local state
SBM-9	1.2	0.2	2.5	0	15	5000	100	bare local state

REFERENCES

(1) Zheng, Q.; Chu, W.; Zhao, C.; Zhang, L.; Guo, H.; Wang, Y.; Jiang, X.; Zhao, J. Ab Initio Nonadiabatic Molecular Dynamics Investigations on the Excited Carriers in Condensed Matter Systems. *WIREs Comput. Mol. Sci.* **2019**, *9*, e1411.

(2) Smith, B.; Akimov, A. V. Modeling Nonadiabatic Dynamics in Condensed Matter Materials: Some Recent Advances and Applications. *J. Phys. Condens. Matter* **2020**, *32*, 073001.

(3) Toutounji, M. Mixed Quantum-Classical Liouville Equation Treatment of Electronic Spectroscopy of Condensed Systems: Harmonic and Anharmonic Electron–Phonon Coupling. *J. Chem. Theory Comput.* **2023**, *19*, 3779–3797.

(4) Kumpulainen, T.; Lang, B.; Rosspeintner, A.; Vauthey, E. Ultrafast Elementary Photochemical Processes of Organic Molecules in Liquid Solution. *Chem. Rev.* **2017**, *117*, 10826–10939.

(5) Alarcos, N.; Cohen, B.; Ziółek, M.; Douhal, A. Photochemistry and Photophysics in Silica-Based Materials: Ultrafast and Single Molecule Spectroscopy Observation. *Chem. Rev.* **2017**, *117*, 13639–13720.

(6) Mai, S.; González, L. Molecular Photochemistry: Recent Developments in Theory. *Angew. Chem. Int. Ed.* **2020**, *59*, 16832–16846.

(7) Blumberger, J. Recent Advances in the Theory and Molecular Simulation of Biological Electron Transfer Reactions. *Chem. Rev.* **2015**, *115*, 11191–11238.

(8) Brunk, E.; Rothlisberger, U. Mixed Quantum Mechanical/Molecular Mechanical Molecular Dynamics Simulations of Biological Systems in Ground and Electronically Excited States. *Chem. Rev.* **2015**, *115*, 6217–6263.

(9) Segatta, F.; Cupellini, L.; Garavelli, M.; Mennucci, B. Quantum Chemical Modeling of the Photoinduced Activity of Multichromophoric Biosystems: Focus Review. *Chem. Rev.* **2019**, *119*, 9361–9380.

(10) Kilina, S.; Kilin, D.; Tretiak, S. Light-Driven and Phonon-Assisted Dynamics in Organic and Semiconductor Nanostructures. *Chem. Rev.* **2015**, *115*, 5929–5978.

(11) Ostroverkhova, O. Organic Optoelectronic Materials: Mechanisms and Applications. *Chem. Rev.* **2016**, *116*, 13279–13412.

(12) Long, R.; Prezhdo, O. V.; Fang, W. Nonadiabatic Charge Dynamics in Novel Solar Cell Materials. *WIREs Comput. Mol. Sci.* **2017**, *7*, e1305.

(13) Dimitriev, O. P. Dynamics of Excitons in Conjugated Molecules and Organic Semiconductor Systems. *Chem. Rev.* **2022**, *122*, 8487–8593.

(14) Liu, X.; Chen, W.; Fang, W; Cui, G. Nonadiabatic Dynamics Simulations for Photoinduced Processes in Molecules and Semiconductors: Methodologies and Applications. *J. Chem. Theory Comput.* **2023**, *19*, 8491–8522.

(15) Beck, M. The Multiconfiguration Time-Dependent Hartree (MCTDH) Method: A Highly Efficient Algorithm for Propagating Wavepackets. *Phys. Rep.* **2000**, *324*, 1–105.

(16) Wang, H.; Thoss, M. Multilayer Formulation of the Multiconfiguration Time-Dependent Hartree Theory. *J. Chem. Phys.* **2003**, *119*, 1289–1299.

(17) Worth, G. A.; Meyer, H.; Köppel, H.; Cederbaum, L. S.; Burghardt, I. Using the MCTDH Wavepacket Propagation Method to Describe Multimode Non-Adiabatic

Dynamics. *Int. Rev. Phys. Chem.* **2008**, *27*, 569–606.
(18) Manthe, U. A Multilayer Multiconfigurational Time-Dependent Hartree Approach for Quantum Dynamics on General Potential Energy Surfaces. *J. Chem. Phys.* **2008**, *128*, 164116.
(19) Tanimura, Y. Stochastic Liouville, Langevin, Fokker–Planck, and Master Equation Approaches to Quantum Dissipative Systems. *J. Phys. Soc. Jpn.* **2006**, *75*, 082001.
(20) Jin, J.; Zheng, X.; Yan, Y. Exact Dynamics of Dissipative Electronic Systems and Quantum Transport: Hierarchical Equations of Motion Approach. *J. Chem. Phys.* **2008**, *128*, 234703.
(21) Shi, Q.; Chen, L.; Nan, G.; Xu, R.; Yan, Y. Efficient Hierarchical Liouville Space Propagator to Quantum Dissipative Dynamics. *J. Chem. Phys.* **2009**, *130*, 084105.
(22) Yan, Y. Theory of Open Quantum Systems with Bath of Electrons and Phonons and Spins: Many-Dissipaton Density Matrixes Approach. *J. Chem. Phys.* **2014**, *140*, 054105.
(23) White, S. R. Density Matrix Formulation for Quantum Renormalization Groups. *Phys. Rev. Lett.* **1992**, *69*, 2863–2866.
(24) Vidal, G. Efficient Simulation of One-Dimensional Quantum Many-Body Systems. *Phys. Rev. Lett.* **2004**, *93*, 040502.
(25) Haegeman, J.; Cirac, J. I.; Osborne, T. J.; Pižorn, I.; Verschelde, H.; Verstraete, F. Time-Dependent Variational Principle for Quantum Lattices. *Phys. Rev. Lett.* **2011**, *107*, 070601.
(26) Li, W.; Ren, J.; Shuai, Z. Numerical Assessment for Accuracy and GPU Acceleration of TD-DMRG Time Evolution Schemes. *J. Chem. Phys.* **2020**, *152*, 024127.
(27) Ren, J.; Li, W.; Jiang, T.; Wang, Y.; Shuai, Z. Time-dependent Density Matrix Renormalization Group Method for Quantum Dynamics in Complex Systems. *WIREs Comput. Mol. Sci.* **2022**, *12*, e1614.
(28) Tully, J. C. Molecular Dynamics with Electronic Transitions. *J. Chem. Phys.* **1990**, *93*, 1061–1071.
(29) Ehrenfest, P. Bemerkung Über die angenäherte Gültigkeit der klassischen Mechanik innerhalb der Quantenmechanik. *Z. Phys.* **1927**, *45*, 455-457.
(30) Akimov, A. V.; Prezhdo, O. V. The PYXAID Program for Non-Adiabatic Molecular Dynamics in Condensed Matter Systems. *J. Chem. Theory Comput.* **2013**, *9*, 4959–4972.
(31) Akimov, A. V.; Prezhdo, O. V. Advanced Capabilities of the PYXAID Program: Integration Schemes, Decoherence Effects, Multiexcitonic States, and Field-Matter Interaction. *J. Chem. Theory Comput.* **2014**, *10*, 789–804.
(32) Barbatti, M.; Ruckenbauer, M.; Plasser, F.; Pittner, J.; Granucci, G.; Persico, M.; Lischka, H. Newton- X : A Surface-hopping Program for Nonadiabatic Molecular Dynamics. *WIREs Comput. Mol. Sci.* **2014**, *4*, 26–33.
(33) Du, L.; Lan, Z. An On-the-Fly Surface-Hopping Program JADE for Nonadiabatic Molecular Dynamics of Polyatomic Systems: Implementation and Applications. *J. Chem. Theory Comput.* **2015**, *11*, 1360–1374.

(34) Weingart, O.; Nenov, A.; Altoè, P.; Rivalta, I.; Segarra-Martí, J.; Dokukina, I.; Garavelli, M. COBRAMM 2.0 — A Software Interface for Tailoring Molecular Electronic Structure Calculations and Running Nanoscale (QM/MM) Simulations. *J. Mol. Model.* **2018**, *24*, 271.
(35) Malone, W.; Nebgen, B.; White, A.; Zhang, Y.; Song, H.; Bjorgaard, J. A.; Sifain, A. E.; Rodriguez-Hernandez, B.; Freixas, V. M.; Fernandez-Alberti, S.; Roitberg, A. E.; Nelson, T. R.; Tretiak, S. NEXMD Software Package for Nonadiabatic Excited State Molecular Dynamics Simulations. *J. Chem. Theory Comput.* **2020**, *16*, 5771–5783.
(36) Furche, F.; Ahlrichs, R.; Hättig, C.; Klopper, W.; Sierka, M.; Weigend, F. Turbomole. *WIREs Comput. Mol. Sci.* **2014**, *4*, 91–100.
(37) Balasubramani, S. G.; Chen, G. P.; Coriani, S.; Diedenhofen, M.; Frank, M. S.; Franzke, Y. J.; Furche, F.; Grotjahn, R.; Harding, M. E.; Hättig, C.; Hellweg, A.; Helmich-Paris, B.; Holzer, C.; Huniar, U.; Kaupp, M.; Marefat Khah, A.; Karbalaei Khani, S.; Müller, T.; Mack, F.; Nguyen, B. D.; Parker, S. M.; Perlt, E.; Rappoport, D.; Reiter, K.; Roy, S.; Rückert, M.; Schmitz, G.; Sierka, M.; Tapavicza, E.; Tew, D. P.; Van Wüllen, C.; Voora, V. K.; Weigend, F.; Wodyński, A.; Yu, J. M. TURBOMOLE: Modular Program Suite for *Ab Initio* Quantum-Chemical and Condensed-Matter Simulations. *J. Chem. Phys.* **2020**, *152*, 184107.
(38) Richter, M.; Marquetand, P.; González-Vázquez, J.; Sola, I.; González, L. SHARC: *Ab Initio* Molecular Dynamics with Surface Hopping in the Adiabatic Representation Including Arbitrary Couplings. *J. Chem. Theory Comput.* **2011**, *7*, 1253–1258.
(39) Mai, S.; Marquetand, P.; González, L. Nonadiabatic Dynamics: The SHARC Approach. *WIREs Comput. Mol. Sci.* **2018**, *8*, e1370.
(40) Avagliano, D.; Bonfanti, M.; Garavelli, M.; González, L. QM/MM Nonadiabatic Dynamics: The SHARC/COBRAMM Approach. *J. Chem. Theory Comput.* **2021**, *17*, 4639–4647.
(41) Valiev, M.; Bylaska, E. J.; Govind, N.; Kowalski, K.; Straatsma, T. P.; Van Dam, H. J. J.; Wang, D.; Nieplocha, J.; Apra, E.; Windus, T. L.; De Jong, W. A. NWChem: A Comprehensive and Scalable Open-Source Solution for Large Scale Molecular Simulations. *Comput. Phys. Commun.* **2010**, *181*, 1477–1489.
(42) Song, H.; Fischer, S. A.; Zhang, Y.; Cramer, C. J.; Mukamel, S.; Govind, N.; Tretiak, S. First Principles Nonadiabatic Excited-State Molecular Dynamics in NWChem. *J. Chem. Theory Comput.* **2020**, *16*, 6418–6427.
(43) Song, H.; Freixas, V. M.; Fernandez-Alberti, S.; White, A. J.; Zhang, Y.; Mukamel, S.; Govind, N.; Tretiak, S. An Ab Initio Multiple Cloning Method for Non-Adiabatic Excited-State Molecular Dynamics in NWChem. *J. Chem. Theory Comput.* **2021**, *17*, 3629–3643.
(44) Lee, I. S.; Ha, J.; Han, D.; Kim, T. I.; Moon, S. W.; Min, S. K. PyUNIxMD: A PYTHON-BASED Excited State Molecular Dynamics Package. *J. Comput. Chem.* **2021**, *42*, 1755–1766.
(45) Shakiba, M.; Smith, B.; Li, W.; Dutra, M.; Jain, A.; Sun, X.; Garashchuk, S.; Akimov, A. Libra: A Modular Software Library for Quantum Nonadiabatic

Dynamics. *Softw. Impacts* **2022**, *14*, 100445.
(46) Yonehara, T.; Hanasaki, K.; Takatsuka, K. Fundamental Approaches to Nonadiabaticity: Toward a Chemical Theory beyond the Born–Oppenheimer Paradigm. *Chem. Rev.* **2012**, *112*, 499–542.
(47) Wang, L.; Akimov, A.; Prezhdo, O. V. Recent Progress in Surface Hopping: 2011–2015. *J. Phys. Chem. Lett.* **2016**, *7*, 2100–2112.
(48) Crespo-Otero, R.; Barbatti, M. Recent Advances and Perspectives on Nonadiabatic Mixed Quantum–Classical Dynamics. *Chem. Rev.* **2018**, *118*, 7026–7068.
(49) Peng J.; Xie Y.; Hu D.; Du L.; Lan Z. Treatment of Nonadiabatic Dynamics by On-The-Fly Trajectory Surface Hopping Dynamics. *Acta Phys.-Chim. Sin.* **2019**, *35*, 28–48.
(50) Wang, L.; Qiu, J.; Bai, X.; Xu, J. Surface Hopping Methods for Nonadiabatic Dynamics in Extended Systems. *WIREs Comput. Mol. Sci.* **2020**, *10*, e1435.
(51) Nelson, T. R.; White, A. J.; Bjorgaard, J. A.; Sifain, A. E.; Zhang, Y.; Nebgen, B.; Fernandez-Alberti, S.; Mozyrsky, D.; Roitberg, A. E.; Tretiak, S. Non-Adiabatic Excited-State Molecular Dynamics: Theory and Applications for Modeling Photophysics in Extended Molecular Materials. *Chem. Rev.* **2020**, *120*, 2215–2287.
(52) Jain, A.; Sindhu, A. Pedagogical Overview of the Fewest Switches Surface Hopping Method. *ACS Omega* **2022**, *7*, 45810–45824.
(53) Schwartz, B. J.; Bittner, E. R.; Prezhdo, O. V.; Rossky, P. J. Quantum Decoherence and the Isotope Effect in Condensed Phase Nonadiabatic Molecular Dynamics Simulations. *J. Chem. Phys.* **1996**, *104*, 5942–5955.
(54) Prezhdo, O. V.; Rossky, P. J. Evaluation of Quantum Transition Rates from Quantum-Classical Molecular Dynamics Simulations. *J. Chem. Phys.* **1997**, *107*, 5863–5878.
(55) Bedard-Hearn, M. J.; Larsen, R. E.; Schwartz, B. J. Mean-Field Dynamics with Stochastic Decoherence (MF-SD): A New Algorithm for Nonadiabatic Mixed Quantum/Classical Molecular-Dynamics Simulations with Nuclear-Induced Decoherence. *J. Chem. Phys.* **2005**, *123*, 234106.
(56) Hack, M. D.; Truhlar, D. G. A Natural Decay of Mixing Algorithm for Non-Born–Oppenheimer Trajectories. *J. Chem. Phys.* **2001**, *114*, 9305–9314.
(57) Zhu, C.; Nangia, S.; Jasper, A. W.; Truhlar, D. G. Coherent Switching with Decay of Mixing: An Improved Treatment of Electronic Coherence for Non-Born–Oppenheimer Trajectories. *J. Chem. Phys.* **2004**, *121*, 7658–7670.
(58) Zhu, C.; Jasper, A. W.; Truhlar, D. G. Non-Born–Oppenheimer Trajectories with Self-Consistent Decay of Mixing. *J. Chem. Phys.* **2004**, *120*, 5543–5557.
(59) Granucci, G.; Persico, M. Critical Appraisal of the Fewest Switches Algorithm for Surface Hopping. *J. Chem. Phys.* **2007**, *126*, 134114.
(60) Xiao, B.; Xu, J.; Wang, L. New Energy-Based Decoherence Correction Approaches for Trajectory Surface Hopping. *Chin. J. Chem. Phys.* **2020**, *33*, 603–612.
(61) Shao, C.; Shi, Z.; Xu, J.; Wang, L. Learning Decoherence Time Formulas for Surface Hopping from Quantum Dynamics. *J. Phys. Chem. Lett.* **2023**, *14*, 7680–

7689.
(62) Jaeger, H. M.; Fischer, S.; Prezhdo, O. V. Decoherence-Induced Surface Hopping. *J. Chem. Phys.* **2012**, *137*, 22A545.
(63) Feng, W.; Xu, L.; Li, X; Fang, W.; Yan, Y. Nonadiabatic Molecular Dynamics Simulation: An Approach Based on Quantum Measurement Picture. *AIP Adv.* **2014**, *4*, 077131.
(64) Xie, B.; Liu, L.; Cui, G.; Fang, W.; Cao, J.; Feng, W.; Li, X. *Ab Initio* Implementation of Quantum Trajectory Mean-Field Approach and Dynamical Simulation of the N2CO Photodissociation. *J. Chem. Phys.* **2015**, *143*, 194107.
(65) Abedi, A.; Maitra, N. T.; Gross, E. K. U. Exact Factorization of the Time-Dependent Electron-Nuclear Wave Function. *Phys. Rev. Lett.* **2010**, *105*, 123002.
(66) Agostini, F.; Min, S. K.; Abedi, A.; Gross, E. K. U. Quantum-Classical Nonadiabatic Dynamics: Coupled- vs Independent-Trajectory Methods. *J. Chem. Theory Comput.* **2016**, *12*, 2127–2143.
(67) Ha, J.; Lee, I. S.; Min, S. K. Surface Hopping Dynamics beyond Nonadiabatic Couplings for Quantum Coherence. *J. Phys. Chem. Lett.* **2018**, *9*, 1097–1104.
(68) Ha, J.; Min, S. K. Independent Trajectory Mixed Quantum-Classical Approaches Based on the Exact Factorization. *J. Chem. Phys.* **2022**, *156*, 174109.
(69) Prezhdo, O. V.; Rossky, P. J. Mean-Field Molecular Dynamics with Surface Hopping. *J. Chem. Phys.* **1997**, *107*, 825–834.
(70) Bai, S.; Xie, W.; Zhu, L.; Shi, Q. Calculation of Absorption Spectra Involving Multiple Excited States: Approximate Methods Based on the Mixed Quantum Classical Liouville Equation. *J. Chem. Phys.* **2014**, *140*, 084105.
(71) Bai, S.; Xie, W.; Shi, Q. A New Trajectory Branching Approximation To Propagate the Mixed Quantum-Classical Liouville Equation. *J. Phys. Chem. A* **2014**, *118*, 9262–9271.
(72) Baskov, R.; White, A. J.; Mozyrsky, D. Improved Ehrenfest Approach to Model Correlated Electron–Nuclear Dynamics. *J. Phys. Chem. Lett.* **2019**, *10*, 433–440.
(73) Xu, J.; Wang, L. Branching Corrected Surface Hopping: Resetting Wavefunction Coefficients Based on Judgement of Wave Packet Reflection. *J. Chem. Phys.* **2019**, *150*, 164101.
(74) Xu, J.; Wang, L. Branching Corrected Mean Field Method for Nonadiabatic Dynamics. *J. Phys. Chem. Lett.* **2020**, *11*, 8283–8291.
(75) Shao, C.; Xu, J.; Wang, L. Branching and Phase Corrected Surface Hopping: A Benchmark of Nonadiabatic Dynamics in Multilevel Systems. *J. Chem. Phys.* **2021**, *154*, 234109.
(76) Li, B.; Xu, J.; Li, G.; Shi, Z.; Wang, L. A Mixed Deterministic–Stochastic Algorithm of the Branching Corrected Mean Field Method for Nonadiabatic Dynamics. *J. Chem. Phys.* **2022**, *156*, 114116.
(77) Li, G.; Shao, C.; Xu, J.; Wang, L. A Unified Framework of Mixed Quantum–Classical Dynamics with Trajectory Branching. *J. Chem. Phys.* **2022**, *157*, 214102.
(78) Li, G.; Shi, Z.; Guo, X.; Wang, L. What Is Missing in the Mean Field Description of Spatial Distribution of Population? Important Role of Auxiliary Wave Packets in Trajectory Branching. *J. Phys. Chem. Lett.* **2023**, *14*, 9855–9863.

(79) Guo, X.; Li, G.; Shi, Z.; Wang, L. Surface Hopping with Reliable Wave Function by Introducing Auxiliary Wave Packets to Trajectory Branching. *J. Phys. Chem. Lett.* **2024**, *15*, 3345–3353.
(80) Broeckhove, J.; Lathouwers, L.; Kesteloot, E.; Van Leuven, P. On the Equivalence of Time-Dependent Variational Principles. *Chem. Phys. Lett.* **1988**, *149*, 547–550.
(81) Lasser, C.; Su, C. Various Variational Approximations of Quantum Dynamics. *J. Math. Phys.* **2022**, *63*, 072107.
(82) Shalashilin, D. V. Quantum Mechanics with the Basis Set Guided by Ehrenfest Trajectories: Theory and Application to Spin-Boson Model. *J. Chem. Phys.* **2009**, *130*, 244101.
(83) Shalashilin, D. V. Nonadiabatic Dynamics with the Help of Multiconfigurational Ehrenfest Method: Improved Theory and Fully Quantum 24D Simulation of Pyrazine. *J. Chem. Phys.* **2010**, *132*, 244111.
(84) Leggett, A. J.; Chakravarty, S.; Dorsey, A. T.; Fisher, M. P. A.; Garg, A.; Zwerger, W. Dynamics of the Dissipative Two-State System. *Rev. Mod. Phys.* **1987**, *59*, 1–85.
(85) Stock, G. A Semiclassical Self-Consistent-Field Approach to Dissipative Dynamics: The Spin–Boson Problem. *J. Chem. Phys.* **1995**, *103*, 1561–1573.
(86) Wang, H. Basis Set Approach to the Quantum Dissipative Dynamics: Application of the Multiconfiguration Time-Dependent Hartree Method to the Spin-Boson Problem. *J. Chem. Phys.* **2000**, *113*, 9948–9956.
(87) Glauber, R. J. Coherent and Incoherent States of the Radiation Field. *Phys. Rev.* **1963**, *131*, 2766–2788.
(88) Sudarshan, E. C. G. Equivalence of Semiclassical and Quantum Mechanical Descriptions of Statistical Light Beams. *Phys. Rev. Lett.* **1963**, *10*, 277–279.
(89) Hillery, M.; O'Connell, R. F.; Scully, M. O. Distribution functions in physics: fundamentals. *Phys Rep*, **1984**, *106*, 121–167.
(90) Shalashilin, D. V.; Child, M. S. Basis Set Sampling in the Method of Coupled Coherent States: Coherent State Swarms, Trains, and Pancakes. *J. Chem. Phys.* **2008**, *128*, 054102.
(91) Makarov, D. E.; Makri, N. Path Integrals for Dissipative Systems by Tensor Multiplication. Condensed Phase Quantum Dynamics for Arbitrarily Long Time. *Chem. Phys. Lett.* **1994**, *221*, 482–491.
(92) Wang, H.; Thoss, M.; Miller, W. H. Systematic Convergence in the Dynamical Hybrid Approach for Complex Systems: A Numerically Exact Methodology. *J. Chem. Phys.* **2001**, *115*, 2979–2990.
(93) Walters, P. L.; Makri, N. Iterative Quantum-Classical Path Integral with Dynamically Consistent State Hopping. *J. Chem. Phys.* **2016**, *144*, 044108.
(94) Cotton, S. J.; Miller, W. H. Symmetrical Windowing for Quantum States in Quasi-Classical Trajectory Simulations: Application to Electronically Non-Adiabatic Processes. *J. Chem. Phys.* **2013**, *139*, 234112.
(95) He, X.; Wu, B.; Shang, Y.; Li, B.; Cheng, X.; Liu, J. New Phase Space Formulations and Quantum Dynamics Approaches. *WIREs Comput. Mol. Sci.* **2022**, *12*, e1619.

(96) Wang, L.; Trivedi, D.; Prezhdo, O. V. Global Flux Surface Hopping Approach for Mixed Quantum-Classical Dynamics. *J. Chem. Theory Comput.* **2014**, *10*, 3598–3605.
(97) Sifain, A. E.; Wang, L.; Prezhdo, O. V. Mixed Quantum-Classical Equilibrium in Global Flux Surface Hopping. *J. Chem. Phys.* **2015**, *142*, 224102.
(98) Qiu, J.; Bai, X.; Wang, L. Subspace Surface Hopping with Size-Independent Dynamics. *J. Phys. Chem. Lett.* **2019**, *10*, 637–644.